

Supplementary information

Intensity-Driven Resurgence of Reverse Saturable Absorption and Vibrational Modes in Hexagonal Silver Nanoplates

Amit Kumar Pradhan^a, Ayon Jyoti Karmakar^a, Sayantan Bhattacharya^{b*}, Suman Kumar^c, Marco Gandolfi^{d,e}, Tara Singha^a, Amiya Priyam^c, Prasanta Kumar Datta^{a*}

^aDepartment of Physics, Indian Institute of Technology Kharagpur, Kharagpur 721302, India

^bCentral Laser Facility, Research Complex at Harwell, Science and Technology Facilities Council, Didcot OX11 0QX, UK.

^cDepartment of Chemistry, School of Physical and Chemical Sciences, Central University of South Bihar, Gaya 824236, India

^dDipartimento di Ingegneria dell'Informazione, Università degli Studi di Brescia, Via Branze 38, 25123 Brescia, Italy

^eConsiglio Nazionale delle Ricerche - Istituto Nazionale di Ottica, Via Branze 45, 25123 Brescia, Italy

*Corresponding Author: Email: pkdatta@phy.iitkgp.ac.in, sayantan.bhattacharya@stfc.ac.uk

Z-scan Technique: The Z-scan technique^{1,2} is used to determine the optical nonlinear absorption (NLA) and nonlinear refraction (NLR) parameters of hexagonal silver nanocrystals (AgNC-550) through open aperture (OA) Z-scan and closed aperture (CA) Z-scan methods, respectively. In the experimental setup, an aqueous solution of NCs contained in a quartz cuvette with an effective path length of 0.2 cm is moved using a translation stage (Newport, GTS150) within the Rayleigh range of a focused Gaussian beam (TEM00). The beam is focused using a convex lens (L1) with a focal length of 20 cm. The experiment utilizes a Libra ultrafast amplifier HE laser system that generates an 808 nm wavelength pulse with a pulse width of approximately 50 fs and a repetition rate of 1 kHz. This laser pumps the Optical Parametric Amplifier (OPA, Topas-Prime), which produces the desired wavelengths for the experiment. Detection is handled by three silicon amplified photodetectors (PDA100A-EC): PD1 for reference, PD2 for the CA configuration, and PD3 for the OA configuration, as illustrated in Figure S1c. PD1 monitors pulse-to-pulse energy variations, serving as a reference signal. The entire experiment and data acquisition process is managed by LabVIEW software. A neutral density filter (ND1) adjusts the input pump power intensity before reaching the sample. Calibration of the Z-scan setup is done by using a standard material like CS₂. All Z-scan measurements are conducted at three excitation wavelengths: 500 nm, 600 nm, and 660 nm, with the beam waists of the focused beam being approximately 38 μm, 40 μm, and 42 μm, respectively. The characterization of Ag NCs in the single-beam Z-scan method involves the employment of a fundamental Gaussian beam; the beam can be defined as;¹

$$I(z,r) = \frac{I_0}{1 + (z/z_r)^2} \exp\left(-\frac{2r^2}{w^2(z)}\right) \exp\left(-\frac{t^2}{\tau_p^2}\right) \quad (1)$$

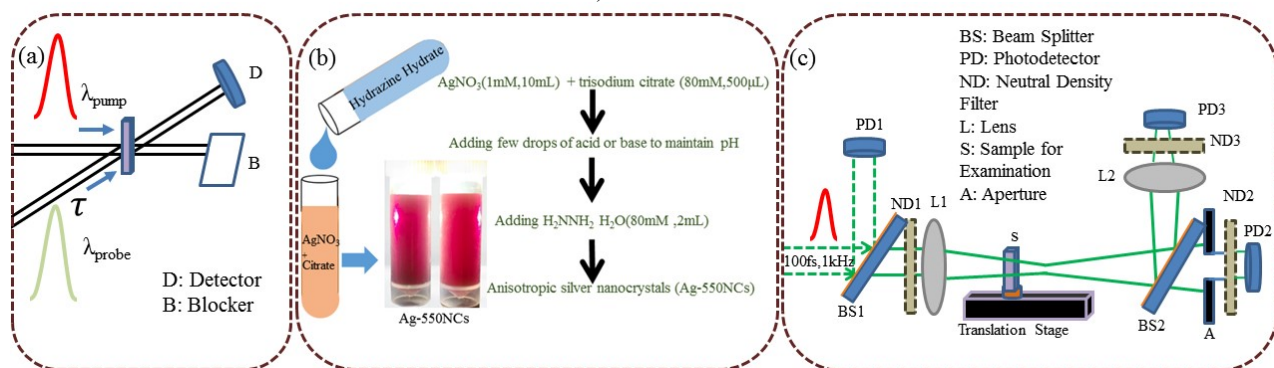


Figure S1. Schematics of (a) pump-probe (transient absorption) spectroscopy (b) sample preparation and (c) illustration of Z-scan experimental assembly

where I_0 is the on-axis intensity at the beam waist (w_0) at focus, z_r is the Rayleigh length, τ_p is the input pulse width. The intensity varies inside the sample while translated in the confocal region, which is given by the as follows,

$$\frac{dI}{dz} = -\alpha(I)I \quad (2)$$

where $\alpha(I)$ is the intensity-dependent nonlinear absorption coefficient, and I is the intensity.

The aqueous NCs solution can be treated as an inhomogeneous broadened system.³ In open aperture (OA) Z-scan, the normalized transmittance traces are well fitted by considering the nonlinear absorption coefficients, including one-photon absorption (1PA), one photon saturation, effective 2PA, and two photon-saturation and 3PA, given by^{3,4}

$$\alpha(I) = \frac{\alpha_0}{\sqrt{1 + \left(\frac{I}{I_{Sat1}}\right)^2}} + \frac{\beta_{eff}I}{\sqrt{1 + \left(\frac{I}{I_{Sat2}}\right)^2}} + \gamma I^2 \quad (3)$$

where, α_0 is the linear absorption coefficient, and β_{eff} is the effective two-photon absorption coefficient, whereas I_{Sat1} and I_{Sat2} are the corresponding saturation intensities for 1PA and 2PA processes. β_{eff} is attributed to both two-photon absorption and successive 1PA occurring in the sample. Here γ is the 3PA coefficient.

Eq. (2) is integrated over the radial direction and time with limit variation from $-\infty$ to $+\infty$ and 0 to ∞ respectively, to fit OA Z-scan traces for NLA parameters extraction.

Transient Absorption Spectroscopy: The ultrafast carrier dynamics of AgNCs-550 nanocrystals are studied using femtosecond transient absorption (TA) spectroscopy (Figure S1a). This technique measures the differential absorption of the sample as a function of the time delay between a pump pulse and a probe pulse, providing the transient absorption spectrum of AgNCs-550. Two specific wavelengths are selected for the pump pulses (blue edge off-resonant pumping: 485 nm and red edge off-resonant pumping: 650 nm). These wavelengths are chosen to excite the localized surface plasmon resonance (LSPR) of the silver nanocrystals (Ag NCs). A broad spectrum of light ranging from 500 nm to 800 nm is used as the probe. This super-continuum is generated by passing light through a sapphire crystal.⁵ The spectrometer records the intensity of the probe light at various delays relative to the pump pulse, capturing how the sample's absorption changes over time.

Structure of AgNCs-550: From transmission electron microscopy (TEM), it is observed that all the silver nanoplates have regular hexagonal shapes and edge lengths of 19.4 ± 3.2 nm, and the average thickness is about 15nm. The statistical plot of edge length is shown in Figure S2(b).

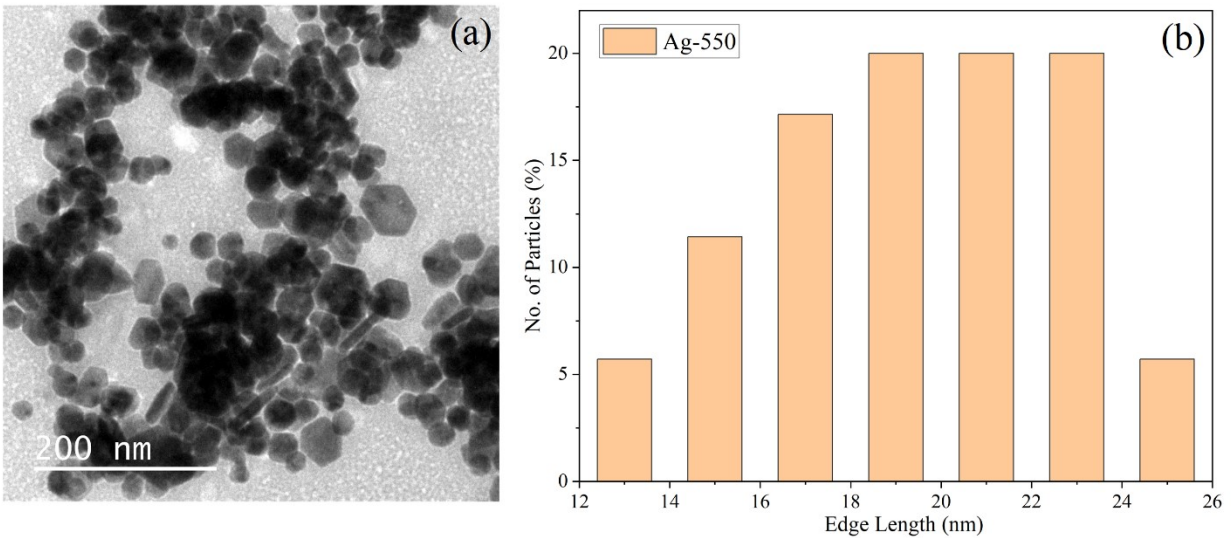


Figure S2: TEM investigation (a) 100nm bar scale, (b) Statistics of sizes of edges of nanoplates.

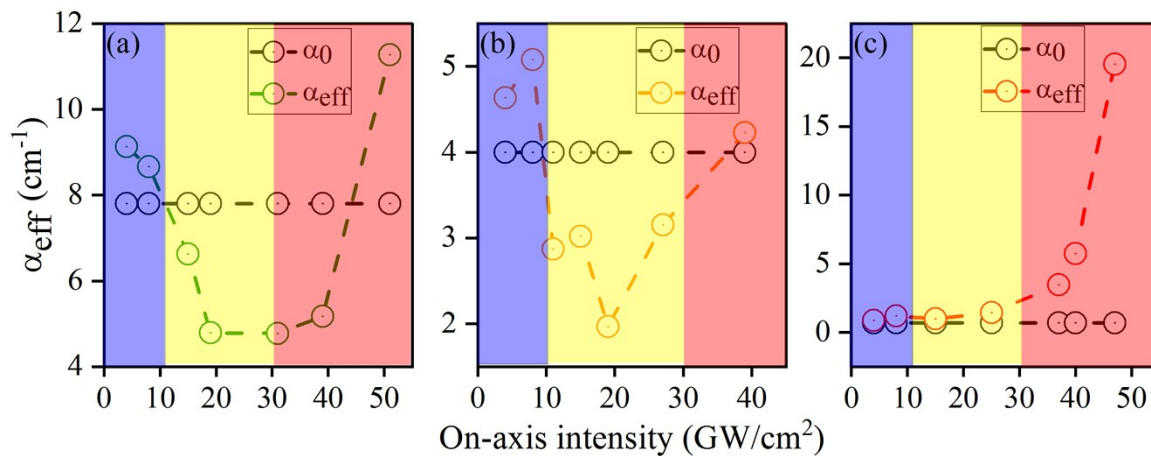


Figure S3. Effective nonlinear absorption coefficients (α_{eff}) for AgNCs-550 at on-axis laser intensities (a) for 550nm excitation, (b) for 600nm excitation and (c) for 660nm excitation.

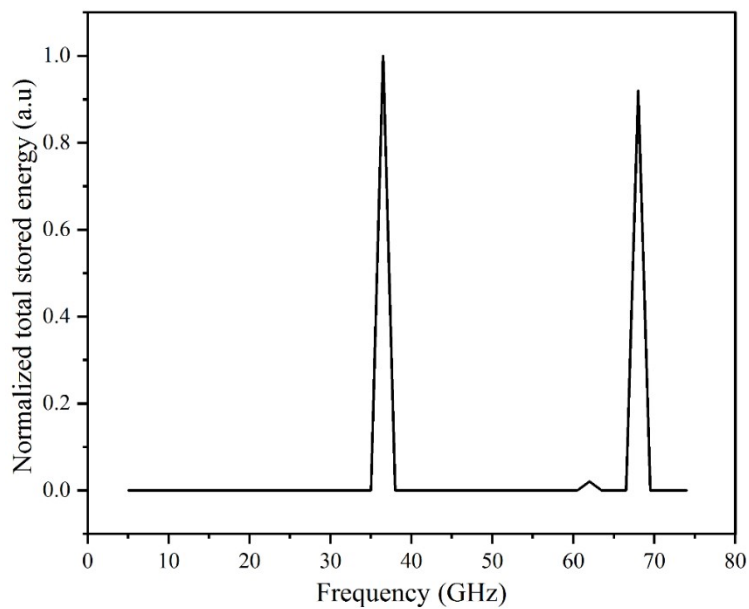


Figure S4: Normalized total stored energy E_m vs mechanical oscillation frequency for AgNCs-550.

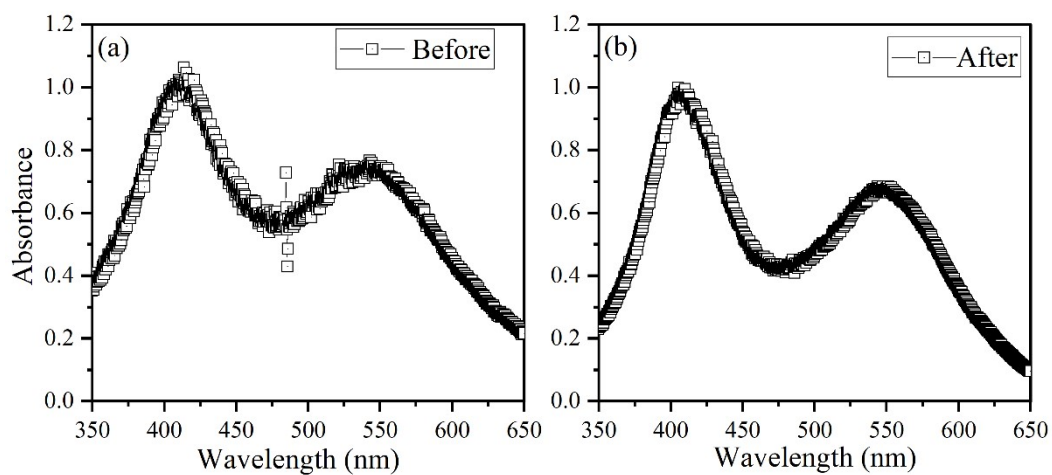


Figure S5: (a,b) Linear absorption of AgNCs-550 before and after TA measurement. (For 650nm excitations, at 12GW/cm²)

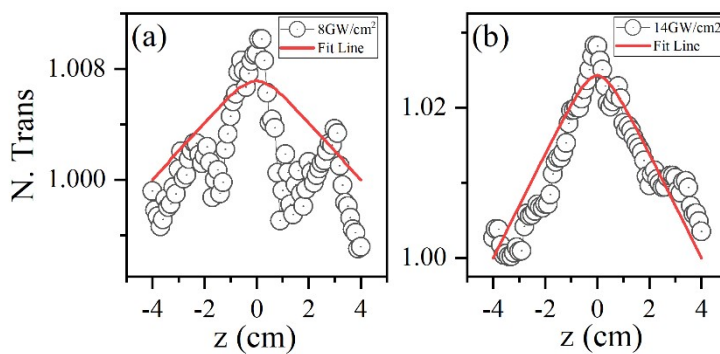


Figure S6: (a,b) NLA: OA normalized transmittance vs z-axis plots for 485nm excitations in AgNCs-550.

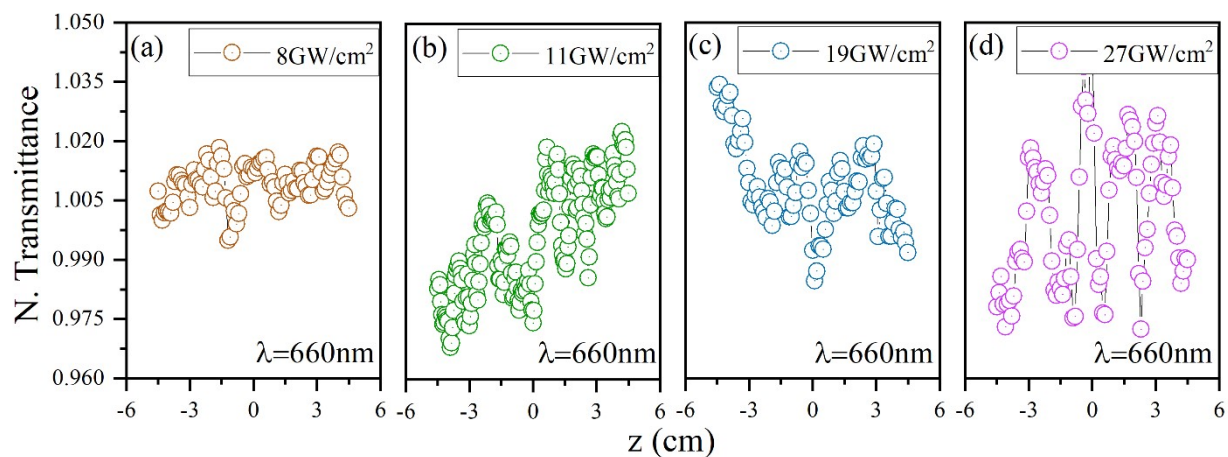


Figure S7: (a-d) are OA Z-scan traces of the solvent (distilled water). The on-axis intensities (8-27GW/cm²) are mentioned at the top of each graph.

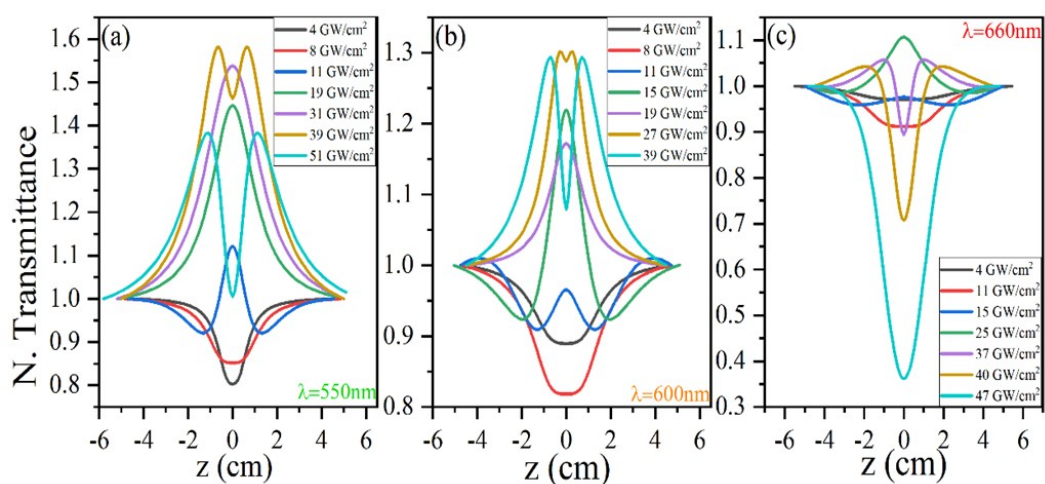


Figure S8: All OA Z-scan traces (experimental fit) for (a) 550nm excitation (b) 600nm excitation, and (c) 660nm excitation.

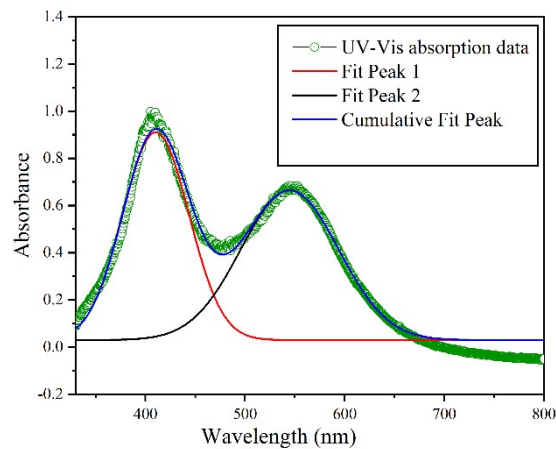


Figure S9: Deconvolution (with Gaussian like functions) of plasmonic absorption for plasmon intensity comparison of AgNCs-550 (see Table-S2).

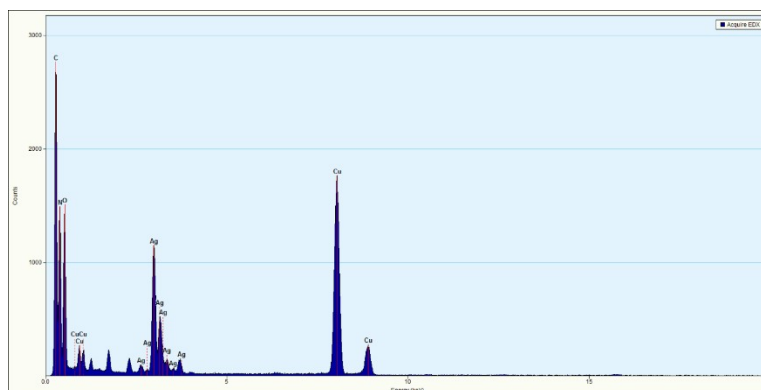


Figure S10: EDX spectrum of silver nanoplates confirming the elemental composition.

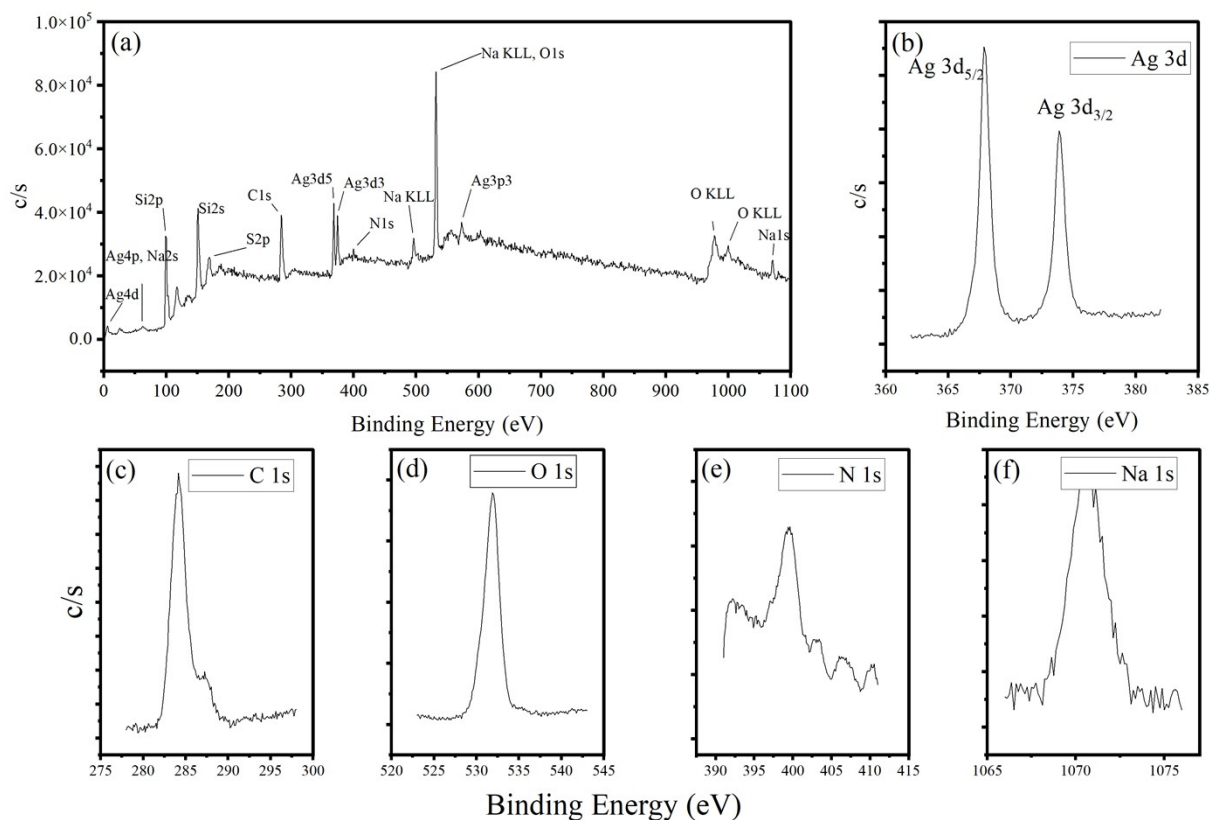


Figure S11: (a) XPS survey spectrum of AgNCs-550; High-resolution XPS spectra of AgNCs-550 for (b) Ag 3d, (c) C 1s, (d) O 1s, (e) N 1s, and (f) Na 1s.

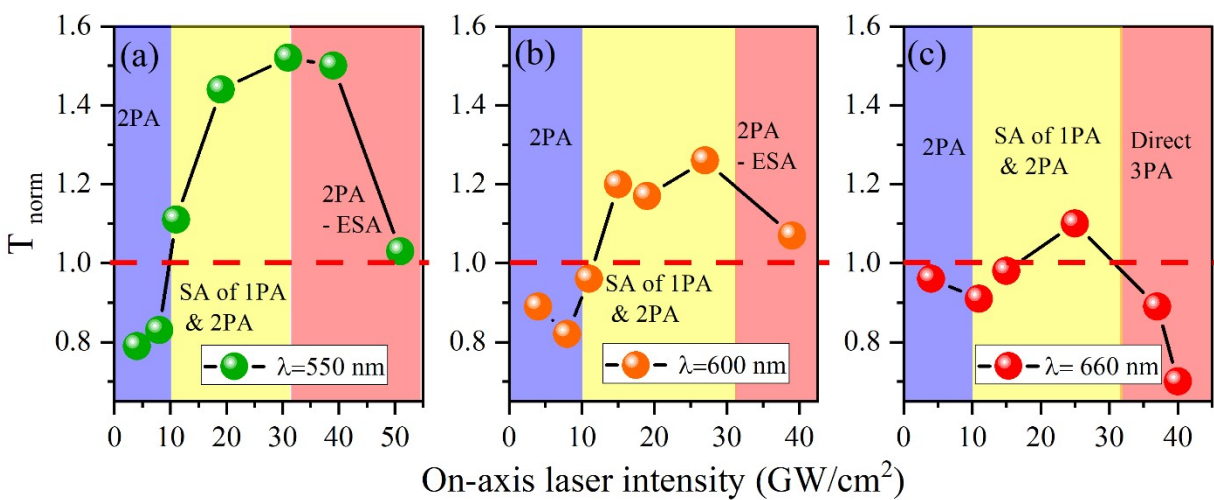


Figure S12: Variation of normalized transmittance as a function of on-axis laser intensity.

nm and thickness of about 20 nm, are used for finite-element modeling (FEM) simulation to show the electric field enhancement on the surface region of nanoplate. The contour plot for electric field values at different excitations (550nm, 600nm, and 660nm) is given in Table S4. Here, we have chosen the Hagemann-defined silver as the material for our simulation. The edge and corner truncation as well as the edge length, is considered while constructing the nanostructure in it. The polarization of the incident electric field (1 V/m) is along the y-axis (perpendicular to one of the octahedral surfaces) to observe the contour electric field.

Moreover, another numerical simulation is also performed using FEM, specifically the Structural Mechanics Module, to match the experimental data with the acoustic modes of silver nanoplates. A frequency domain study is conducted utilizing the external stress 1N/m^2 . The shapes and dimensions of the samples are based on experimental data obtained from TEM. Each structure is meshed with a fine, physics-controlled mesh. The mechanical properties of silver are defined using bulk values: Young's modulus at 50 GPa, Poisson's ratio at 0.3, and density at 7900 kg/m^3 . The deformations in AgNCs-550 say it shows two vibrational modes (I & II) have 36.5GHz frequency and 68GHz frequency, respectively.

Explaining transmittance in NLA: All OA Z-scan traces of AgNCs-550 are explained by considering the nature of transmittance (Figure S8). At low laser intensity, transmittance is decreased at the beam waist due to RSA, which is contributed by two-photon absorption(2PA). In the Table-S1 it is represented as Type-I. The W-shaped transmittance traces are represented as Type-II, where transmittance increased at the beam waist due to 2PA saturation. In Type-III (inverted V-shaped) traces, the transmittance curve is dominated by both one-photon absorption(1PA) and 2PA saturation. The valley formation in NLA traces is due to 2PA-assisted ESA and three-photon absorption(3PA), which is denoted as Type-IV (M-shaped traces). In Type-V, there is no sign of optical transparency due to higher-order NLA. Between 550nm and 600nm excitation, 550nm is more dominated by the saturation of absorption. At 660nm excitation, it is dominated by 3PA, for which it gives a Type-V trace.

Table S1: Different types of NLA traces (for 550nm,600nm, and 660nm excitation).

Intensity(GW/cm ²)	550nm	Intensity(GW/cm ²)	600nm	Intensity(GW/cm ²)	660nm
4	Type-I	4	Type-I	4	Type-I
8	Type-I	8	Type-I	11	Type-I
11	Type-II	11	Type-II	15	Type-II
19	Type-III	15	Type-II	25	Type-II
31	Type-III	19	Type-III	37	Type-IV
39	Type-IV	27	Type-IV	40	Type-IV
51	Type-IV	39	Type-IV	47	Type-V

Table S2: Details of Gaussian deconvolutions of AgNCs-550 (*area under the deconvoluted peak)

Table S3: NLA coefficients extracted from OA Z-scan data in 550nm, 600nm, and 660nm excitation. Here I_0 is the on-axis intensity.

Wavelength (nm)	I_0 (GW/cm ²)	I_{sat1} (GW/cm ²) ± 0.01	β_{eff} (cm/GW) ± 0.03	I_{sat2} (GW/cm ²) ± 0.04	γ (cm ³ /GW ²) ± 0.0001	
550	4	---	01.83	0.74	---	
	8	---	01.69	0.51	---	
	11	0.57	05.42	0.91	---	
	19	0.20	07.40	0.54	---	
	31	0.20	08.30	0.50	---	
	39	0.20	06.20	0.50	0.0010	
	51	0.15	08.90	0.43	0.0027	
600	4	---	02.51	0.25	---	
	8	---	04.29	0.25	---	
	11	0.01	12.91	0.19	---	
	15	0.15	13.11	0.20	---	
	19	0.03	12.11	0.15	---	
	27	0.18	09.12	0.23	0.0010	
	39	0.19	10.11	0.24	0.0017	
660	4	---	01.36	0.12	---	
	11	---	04.06	0.12	---	
	15	0.10	06.39	0.15	---	
	25	0.90	13.05	0.10	---	
	37	1.01	12.04	0.13	0.0013	
	40	1.00	09.84	0.10	0.0029	
	47	1.00	08.84	0.10	0.0084	
SPR Peak 1			SPR Peak 2			Ratio of Plasmon intensities ASPR1/ASPR2
Position (nm)	FWHM (nm)	Integrated intensity* ASPR1	Position (nm)	FWHM (nm)	Integrated intensity* ASPR2	
~410	78.31	73.36	~550	115.58	78.02	

Table S4: The contour

electric field in AgNCs-550.

Wavelength (nm)	Contour Electric field (V/m)*10 ⁻¹
(i)550	7.2
(ii)600	7.0
(iii)660	6.6

Table S5: Intensity(I₀) vs. ΔT (transmittance change) and Intensity(I₀) vs. n₂ for different excitation(550nm,600 and 660nm) in CA Z-scan. .Here Δφ is the phase shift due to NLA.

Wavelength (nm)	I ₀ (GW/cm ²)	~ΔT	n ₂ × 10 ⁻⁶ (cm ² /GW)	Δφ(×10 ⁻³)
550	44	0.4	0.99±0.03	----
	63	1.25	2.13±0.05	----
	68	1.28	1.87±0.05	----
600	25	0.06	0.34±0.01	----
	37	0.1	0.32±0.01	----
	41	1.2	0.33±0.01	----
660	18	0.32	2.33±0.09	----
	28	0.58	2.63±0.03	----
	36	0.95	2.99±0.04	-52.82±10

Reference:

- [1] Sheik-Bahae, M., Said, A. A., Wei, T. H., Hagan, D. J., & Van Stryland, E. W. (1990). Sensitive measurement of optical nonlinearities using a single beam. *IEEE journal of quantum electronics*, 26(4), 760-769.
- [2] Sheik-Bahae, M., Said, A. A., & Van Stryland, E. W. (1989). High-sensitivity, single-beam n₂ measurements. *Optics letters*, 14(17), 955-957.
- [3] Jiang, J., Zuo, S., Wang, G., Liu, J., Zhang, X., & Gao, Y. (2022). Double transformation of the nonlinear absorption in silver nanoparticles. *Optics Express*, 30(23), 41255-41263.

- [4] Reyna, A. S., Russier-Antoine, I., Bertorelle, F., Benichou, E., Dugourd, P., Antoine, R., ... & de Araújo, C. B. (2018). Nonlinear refraction and absorption of Ag₂₉ nanoclusters: evidence for two-photon absorption saturation. *The Journal of Physical Chemistry C*, 122(32), 18682-18689.
- [5] Prodhan, S., Chauhan, K. K., Singha, T., Karmakar, M., Maity, N., Nadarajan, R., ... & Datta, P. K. (2023). Comprehensive excited state carrier dynamics of 2D selenium: One-photon and multi-photon absorption regimes. *Applied Physics Letters*, 123(2).